Multi-objective Dynamic Reconfiguration for Urban Distribution Network Considering Multi-level Switching Modes

Hongjun Gao, Wang Ma, Yingmeng Xiang, Zao Tang, Xiandong Xu, Hongjin Pan, Fan Zhang, and Junyong Liu

***Abstract*—The increasing integration of photovoltaic generators (PVGs) and the uneven economic development in different regions may cause the unbalanced spatial-temporal distribution of load demands in an urban distribution network (UDN). This may lead to undesired consequences, including PVG curtailment, load shedding, and equipment inefficiency, etc. Global dynamic reconfiguration provides a promising method to solve those challenges. However, the power flow transfer capabilities for different kinds of switches are diverse, and the willingness of distribution system operators (DSOs) to select them is also different. In this paper, we formulate a multi-objective dynamic reconfiguration optimization model suitable for multi-level switching modes to minimize the operation cost, load imbalance, and the PVG curtailment. The multi-level switching includes feeder-level switching, transformer-level switching, and substation-level switching. A novel load balancing index is devised to quantify the global load balancing degree at different levels. Then, a stochastic programming model based on selected scenarios is established to address the uncertainties of PVGs and loads. Afterward, the fuzzy *c*-means (FCMs) clustering is applied to divide the time periods of reconfiguration. Furthermore, the modified binary particle swarm optimization (BPSO) and Cplex solver are combined to solve the proposed mixed-integer second-order cone programming (MISOCP) model. Numerical results based on the 148-node and 297-node systems are obtained to validate the effectiveness of the proposed method.**

***Index Terms*—Binary particle swarm optimization (BPSO), dynamic reconfiguration, multi-level switching, mixed-integer second-order cone programming (MISOCP), urban distribution network (UDN).**

NOMENCLATURE

$\gamma(j)$	Set of transformers at substation node j
$\alpha(j,f)$	Set of feeders for transformer f at substation node j
$\alpha(j)$, $\beta(j)$	Sets of nodes whose parent and child are node j
ω	Inertia weight of BPSO algorithm
$\delta_{ij,t}^{\mathrm{sw,in}}$	Binary variable, and $\delta_{ij,t}^{\mathrm{sw,in}}$ equals 1 if status of switch branch ij changes from open to close at time period t
$\delta_{ij,t}^{\mathrm{sw,de}}$	Binary variable, and $\delta_{ij,t}^{\mathrm{sw,in}}$ equals 1 if status of switch branch ij changes from close to open at time period t
A^{PV}	Photovoltaic generators (PVGs) curtailment
B	Set of nodes
B^{sub}, B^{PV}	Sets of nodes connected with substation and photovoltaic (PV) generator
B_t^{sub}, B_t^{trans}, B_t^{feed}	Substation, transformer, and feeder load balancing indexes at time period t
$B_{j,f,t}^{\mathrm{feed}}$	Feeder load balancing index of transformer f for substation node j at time period t
$B_{j,t}^{\mathrm{trans}}$	Transformer load balancing index for substation node j at time period t
c^{loss}, c_t^{sub}, c^{lr}	Prices for power loss, main grid power, and load shedding
C^{loss}, C^{sub}, C^{lr}	Costs for power loss, main grid power, and load shedding
c_1, c_2	Learning factors of BPSO algorithm
$c_{ij}^{\mathrm{sw,sect}}$, $c_{ij}^{\mathrm{sw,feed}}$, $c_{ij}^{\mathrm{sw,trans}}$, $c_{ij}^{\mathrm{sw,sub}}$	Switching costs for sectionalizing switch, feeder tie switch, transformer tie switch, and substation tie switch
$d_{c,t}$	Euclidean distance between point $\boldsymbol{X}_t$ and cluster $\boldsymbol{V}_c$
E, $E^{\mathrm{sw,sect}}$, E^{sw}	Sets of branches, sectionalizing switch branches, and switch branches
E^{always}	Number of unadjustable branches

Manuscript received: December 18, 2020; revised: March 28, 2021; accepted: June 10, 2021. Date of corscheck: Date of CrossCheck: June 10, 2021. Date of online publication: July 27, 2021.

This work was supported by the National Key R&D Program of China (No. 2019YFE0123600), National Natural Science Foundation of China (No. 52077146), and Young Elite Scientists Sponsorship Program by CSEE (No. CESS-YESS-2019027).

H. Gao, W. Ma (corresponding author), Z. Tang, H. Pan, F. Zhang, and J. Liu are with the College of Electrical Engineering, Sichuan University, Chengdu 610065, China (e-mail: gaohongjun@scu.edu.cn; 2210208279@qq.com; tangzaoscu@163.com; 837400851@qq.com; 1341934500@qq.com; liujy@ scu.edu.cn).

Y. Xiang is with Iowa State University, Ames, Iowa, 50010, USA (e-mail: yingmengxiang@gmail.com).

X. Xu is with the Key Laboratory of Smart Grid of Ministry of Education, Tianjin University, Tianjin 300072, China (e-mail: xuxiandong@tju.edu.cn).

DOI: 10.35833/MPCE.2020.000870

$E^{\text{sw, feed}}$, $E^{\text{sw, trans}}$, $E^{\text{sw, sub}}$	Sets of feeders, transformers, and substation tie switch branches
f	Index of transformers at substation node j
f_s	Probability of scenario s
g_j, b_j	Conductance and susceptance from node j to ground
i, j	Indexes of nodes
ij, jk	Indexes of branches
$\underline{I}_{ij}$, $\bar{I}_{ij}$	Upper and lower bounds of current for branch ij
$\hat{I}_{ij,t}$, $\hat{V}_{j,t}$	Square current of branch ij and square voltage of node j at time period t, and the symbol $\hat{}$ denotes the linearization of power flow constraints
k	Index of feeders for transformer f at substation node j
M	A "big-M"-type constant
N^{sub}, N^{trans}	Number of substations and transformers
N_j^{trans}	Number of transformers connected to substation node j
$N_{j,f}^{\text{feed}}$	Number of feeders connected to transformer f at substation node j
$N_{ij}^{\text{sw, max}}$	The maximum regulation number of switch on branch ij
N_s	Number of scenarios
N^{sw}	Number of switches, which varies among multi-level switching modes
N^{swr}	Coding length in each reconfiguration time period, which is equal to the number of switches contained in all the loops
$\boldsymbol{p}_{im}^n$	Individual optimal position of the i^{th} particle in the n$^{\text{th}}$ iteration
$\boldsymbol{p}_{gm}^n$	Global optimal position in the n^{th} iteration
$P_j^{\text{sub, max}}$	Upper bound of substation active power at node j
$P_{ij}^{\max}$	Upper bound of active power for branch ij
$P_{j,f}^{\text{trans, max}}$, $P_{j,f}^{\text{trans, min}}$, $Q_{j,f}^{\text{trans, max}}$, $Q_{j,f}^{\text{trans, min}}$	Upper and lower bounds of active and reactive power for transformer f at substation node j
$P_{j,t}^{\text{sub}}$, $Q_{j,t}^{\text{sub}}$, $R_{j,t}^{\text{sub}}$	Active power, reactive power, and load rate for substation node j at time period t
$P_{j,f,t}^{\text{trans}}$, $Q_{j,f,t}^{\text{trans}}$, $R_{j,f,t}^{\text{trans}}$	Active power, reactive power, and load rate of transformer f for substation node j at time period t
$P_{j,t}^{\text{PV}}$, $P_{j,t}^{\text{PV, ava}}$	Active power and available active power for PV node j at time period t
$P_{j,t}$, $Q_{j,t}$	Active power injection and reactive power injection for node j at time period t
$P_{ij,t}$, $Q_{ij,t}$	Active power flow and reactive power flow from node i to node j at time period t
$P_{j,t}^{\text{l}}$, $Q_{j,t}^{\text{l}}$	Active power demand and reactive power demand for load node j at time period t
$P_{j,t}^{\text{lr}}$, $Q_{j,t}^{\text{lr}}$	Active power reduced and reactive power reduced for load node j at time period t
q	Index of location number for natural sorting of switch branches in all loops
r_{ij}, x_{ij}	Resistance and reactance of branch ij
$R_t^{\text{sub, avr}}$	Average load rate of substations at time period t
$R_{j,t}^{\text{trans, avr}}$	Average load rate of transformers for substation node j at time period t
$R_{jk,t}^{\text{feed}}$	Load rate of feeder jk at time period t
$R_{j,f,t}^{\text{feed, avr}}$	Average load rate of feeders for transformer f in substation node j at time period t
s	Index of scenarios
t	Index of time periods
$u_{c,t}^b$	Membership degree of point $\boldsymbol{X}_t$ to cluster $\boldsymbol{V}_c$
$\boldsymbol{U}_{C\times T}$	Fuzzy membership matrix
$\boldsymbol{V}$	Cluster centers
$\boldsymbol{V}^k$	Cluster centers in the k^{th} iteration
$\boldsymbol{v}_{im}^n$	Velocity of the i^{th} particle in the n^{th} iteration
$\hat{V}_{j,t}$, $\hat{V}_{i,t}$	Square voltage of node i and node j at time period t
$w_{ij,t}$	Operation state of switch branch ij at time period t (binary variable)
$\boldsymbol{x}$	First-stage decision variables
$\boldsymbol{X}_t$	Spatial distribution of load demand at time period t
$\boldsymbol{y}_{\text{s}}$	Second-stage decision variables
$(\bullet)^*$	Dummy variable for connectivity constraints

I. Introduction

UNCERTAINTIES of load growth and photovoltaic generator (PVG) installation may lead to the power generation-consumption unbalance, and further result in PVG curtailment, load shedding, or equipment inefficiency, etc. This is a typical situation in most urban distribution networks (UDNs), which requires certain spatial-temporal flexibility. Switch reconfiguration is an effective measure in providing the desired flexibility. However, traditional discorded switching mode cannot take full advantage of switches due to the heavy reliance on the human experience. In the existing research works, the reconfiguration methods of UDN can be classified into two types [1], [2]: ① static reconfiguration, which controls the switches manually to find out an improved fixed topology for a yearly/seasonal operation; ② dynamic reconfiguration, which controls the switches remotely and automatically to remove the grid congestion for real-time operation. Nevertheless, the static reconfiguration cannot satisfy the temporal flexibility under the unbalanced spatial-temporal distribution of load demands in the UDN, while the dynamic reconfiguration can show better performance by changing

the network topology several times in the scheduling time horizon. In addition, some switches link the feeders under the same transformer while others connect the feeders under different transformers or substations. Those switches are installed at three hierarchies (feeder, transformer, and substation) with different capabilities in transferring the power flows in the UDN. Thus, multi-level (feeder-level, transformer-level, substation-level) dynamic reconfiguration method is necessary to cope with the risk brought by large-scale power flow regulation and fully utilize the transfer capabilities of these switches for the UDN under different unbalanced distributions of power generations and demands.

Network reconfiguration has been extensively studied, which aims to reduce the power loss, improve the voltage quality and load balancing of distribution networks with high penetration of distributed generations (DGs) [3] - [6]. Meanwhile, the reconfiguration optimization model is changing from single-objective type to multi-objective type [7]. A multi-objective reconfiguration model was proposed in [8] to minimize the active power loss, load imbalance, and the maximum node voltage deviation index simultaneously, considering the variabilities of loads and DGs. In [9], a novel voltage volatility index was devised to incorporate the impact of different distribution network parameters. Since it could directly characterize the influence of network topology on the voltage volatility, the potential of network reconfiguration in mitigating the voltage volatility was tapped correctly. In [10], a distribution network reconfiguration model was formulated to minimize the random fuzzy expected value of active power loss and maximum probability of voltage limits, with random-fuzzy uncertainties of both DGs and loads taken into account. However, those studies rarely regarded the DG curtailment as the optimization target in the research of network reconfiguration. Moreover, the unbalanced distribution of load demands in UDNs will also decrease DG consumption. To address this issue, minimizing DG curtailment should be incorporated into the objectives of network reconfiguration. In [11], a state-based sequential network reconfiguration strategy was presented by the Markov decision process to minimize renewable DG curtailment and load shedding. A two-stage robust dynamic reconfiguration model with a small number of critical switches changing the statuses was established in [12]. The results showed that DG curtailment was significantly reduced by only a few times of reconfiguration per day. It is well known that two feeders are linked with each other by the tie switches, which are normally open. Those feeders may be from the same transformer, different transformers or even different substations. The power flow transfer capabilities are different for different categories of tie switches. The existing studies did not fully explore those features and their operation limits. To make it clearer, we divide those tie switches into feeder tie switch, transformer tie switch and substation tie switch. Especially, transformer tie switch is defined as the one that links two feeders from different transformers while substation tie switches are those that link two feeders from different substations. Almost all the distribution system operators (DSOs) prefer to regulate the feeder tie switches in the network reconfiguration as long as the expected target can be roughly achieved by their transfer capabilities. Especially, the increasing benefits brought by more switches (transformer tie switches and substation tie switches) may be so slight in some cases. In this regard, multi-level (feeder-level, transformer-level, and substation-level) switching modes associated with the participation by different tie switches play an essential role in the realistic dynamic reconfiguration of UDNs.

It is usually difficult to solve the dynamic configuration problem with nonlinear power flow equations and numerous binary variables of switches. Existing algorithms can be categorized into three groups: traditional analytical algorithms [13], [14], heuristic algorithms, e.g., branch exchange [15], [16], and intelligence optimization algorithm, e.g., genetic algorithm and particle swarm optimization [17], [18]. Although traditional optimization algorithms can give the global solution, it is subject to the curse of dimensionality when applied to large-scale networks. Heuristic algorithms have relatively poor performance in calculation and global search. The intelligence optimization algorithm may be easily trapped in local optimization. Therefore, the traditional analytical algorithm and intelligence optimization algorithm can be combined to speed up the solution. The second-order cone programming (SOCP) [19] is widely applied to transform the dynamic reconfiguration model into a mixed-integer second-order cone programming (MISOCP) problem. Then, the modified model can be solved by the combinational method of modified binary particle swarm optimization (BPSO) and Cplex. BPSO works better in complex binary problems. Cplex solver can be used to find out the optimal solution. Moreover, the time-period division for the dynamic reconfiguration is necessary to reduce the dimension of binary variables during a large scheduling time horizon.

Based on the foregoing discussions, this paper proposes a multi-objective dynamic reconfiguration model considering multi-level switching modes, aiming at minimizing the economic operation cost, load imbalance, and PVG curtailment of UDNs. Different from the existing researches, the proposed multi-level switching mode is set according to the participation by different tie switches located at the feeder-level, transformer-level, and substation-level. Firstly, three power flow transfer means corresponding to those different switching modes are presented in detail. Secondly, a deterministic multi-objective dynamic reconfiguration model considering load balancing is formulated by applying the above multi-level switching modes. The load balancing index is defined to judge the balance degree at different levels of UDN, while diverse switching price and operation limits are modeled for the tie switches at different levels. Thirdly, a stochastic programming model based on scenario set is formulated to address the uncertainties of PVG output and load demand, in which the fuzzy *c*-means (FCM) clustering [20] is introduced to divide the time periods of reconfiguration to solve the problem efficiently. Fourthly, the BPSO and Cplex solver work together to solve the proposed reconfiguration model. Finally, the 148-node and 297-node UDNs are used

to demonstrate the effectiveness of the proposed method.

Specially, the main contributions of this paper are twofold. Firstly, dynamic reconfiguration considering multi-level switching mode is proposed to meet the spatial-temporal flexibility required by the unbalanced distribution of power generations and demands. Thus, an appropriate switching mode can be optimized to avoid the large-scale power flow regulations with low incremental benefit. Secondly, the nonlinear dynamic reconfiguration model is transformed into a MISOCP problem, which is solved by the proposed combinational algorithm. The second-order cone relaxation of load balancing index and power flow in this paper is proven to be accurate.

The rest of the paper is organized as follows. Section II describes three power flow transfer means as the preliminaries for the subsequent multi-level switching modes. The deterministic multi-objective dynamic reconfiguration model suitable for multi-level switching modes is presented in Section III. Section IV formulates a stochastic programming model based on the selected scenarios. FCM and the combinational solution method consisting of BPSO and Cplex are presented in Section V. Case studies about UDN reconfiguration considering multi-level switching modes are conducted in Section VI. Finally, conclusions are drawn in Section VII.

II. Three Power Flow Transfer Means

A typical 10 kV UDN is a layered topology composed of three levels, i. e., feeder-level, transformer-level, and substation-level. It is well known that all feeders are usually linked with each other by the tie switches no matter those feeders are from the same transformer, different transformers, or different substations. But power flow transfer capability is different when regulating different switches. Those power flow transfer behaviors are defined as feeder-transfer, transformer-transfer, and substation-transfer, respectively, which can achieve the network reconfiguration goal by executing the commands according to DSOs. Since the proposed multi-level switching modes are related to the participation of different tie switches, it is necessary to illustrate those three transfer means in detail.

A. Feeder-transfer

Feeder-transfer is to transfer the load to other feeders under the same transformer or bus by regulating the tie switches and sectionalizing switches. As shown in Fig. 1, both the feeder S1T11 and feeder S1T12 are supplied by the secondary side of the transformer S1T1. Load demand in block 1 can be transferred between the two feeders via changing the on/off statuses of BS2, BS3, and FS1. There are three active switch combinations: ① BS2 and BS3 on, FS1 off; ② FS1 and BS2 on, BS3 off; ③ FS1 and BS3 on, BS2 off. In comparison, block 2 only has two combinations: BS1 or FS2 on.

B. Transformer-transfer

Transformer-transfer is to transfer the load to other feeders under different transformers in the same substation. The low-voltage side of the transformers in a 110 kV substation usually adopts a sectionalized single-bus configuration.

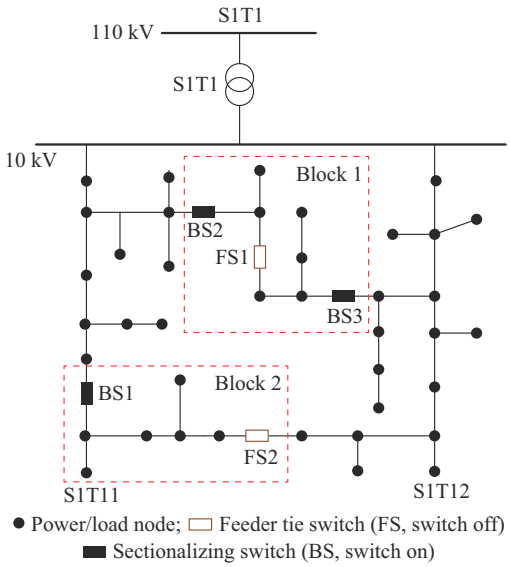

Fig. 1. Topology of feeder-transfer.

Additionally, the sectionalized operation is used under the normal condition to hedge against possible short-circuit current. As shown in Fig. 2, transformers S1T1 and S1T2 are operated in the split mode. Two feeders (S1T12, S1T21) belonging to different transformers have a load shift by changing the on/off status of transformer tie switch TS1 and sectionalizing switch, i.e., the transformer-transfer between S1T1 and S1T2.

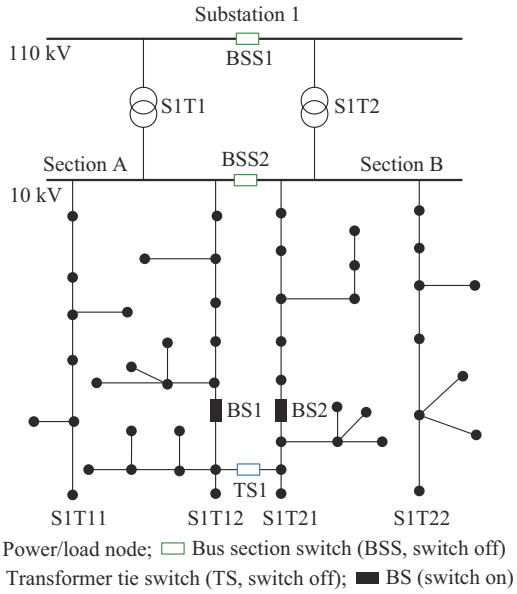

Fig. 2. Topology of transformer-transfer.

C. Substation-transfer

Substation-transfer is to transfer the load to other feeders belonging to a different substation. As shown in Fig. 3, feeders S1T11 (in substation 1) and S2T11 (in substation 2) are linked with each other via the substation tie switch SS3. Furthermore, in block 2, the substation-transfer between substation 1 and substation 2 can be realized by adjusting the operating statuses of SS1, SS2, BS4, and BS1.

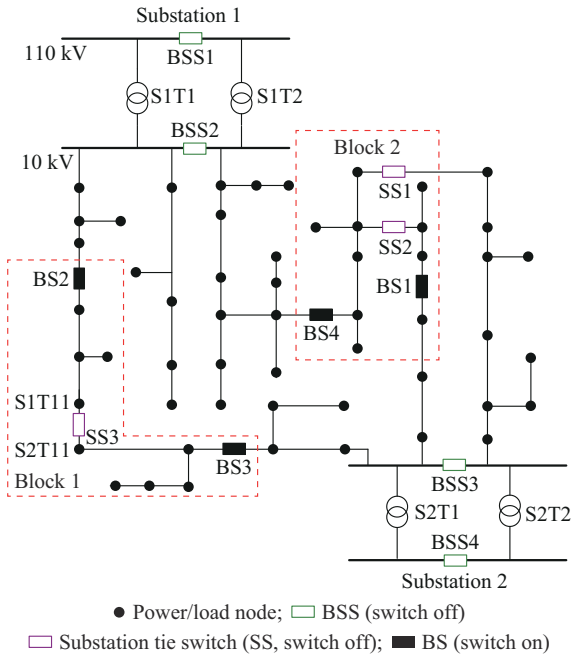

Fig. 3. Topology of substation-transfer.

III. Deterministic Multi-objective Dynamic Reconfiguration Model Suitable for Multi-level Switching Modes

As shown in Table I, only feeder tie switches are involved in the feeder-level reconfiguration. At the transformer-level, both the transformer tie switches and feeder tie switches are taken into account.

TABLE I
Multi-level Switching Modes

Switching mode	Tie switch			Transfer mean		
	FS	TS	SS	Feeder-transfer	Transformer-transfer	Substation-transfer
Feeder-level	√	×	×	√	×	×
Transformer-level	√	√	×	√	√	×
Substation-level	√	√	√	√	√	√

Note: √ means included; × means not included.

Naturally, all the switches are involved in the substation-level reconfiguration, which is the same as the general global reconfiguration. A deterministic multi-objective dynamic reconfiguration model is proposed in this section. Note that the above three reconfiguration strategies do not need to be modeled separately. Different multi-level switching decisions can be realized by adjusting the candidate switch set and the parameters in the functions/constraints in the following model.

A. Multi-level Equivalent Output for Substation

In this paper, the power loss of transformers is neglected. Then, the equivalence of the 110 kV substation can be illustrated in the right part of Fig. 4. Specifically, the output power for the substation 1 can be expressed as the summation of power flow in all four branches linked to substation 1 while the active power for transformer S1T1 P^{S1T1} is equal to the sum of power demand of feeder S1T11 P_{11} and power demand of feeder S1T12 P_{12}. The feeder power is equivalent to the power flow in the corresponding branch.

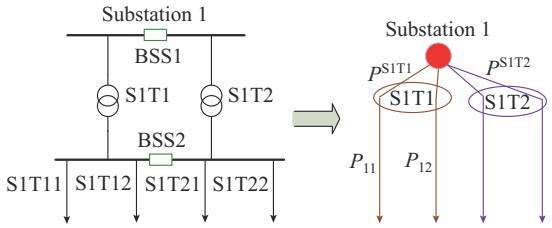

Fig. 4. 110 kV substation node equivalence.

B. Objective Functions

1) Economic Operation Cost

Apart from the network power loss cost, the electricity purchasing cost from the main grid, switching cost, and load shedding cost are all included in the operation cost.

$$\min f_1 = C^{\mathrm{loss}} + C^{\mathrm{sub}} + C^{\mathrm{sw}} + C^{\mathrm{lr}} \tag{1}$$

$$C^{\mathrm{loss}} = \sum_{t\in T}\Delta t \sum_{ij\in E} c^{\mathrm{loss}} r_{ij} I_{ij}^{\wedge} \tag{2}$$

$$C^{\mathrm{sub}} = \sum_{t\in T}\Delta t \sum_{j\in B^{\mathrm{sub}}} c_t^{\mathrm{sub}} P_{j,t}^{\mathrm{sub}} \tag{3}$$

$$\begin{aligned} C^{\mathrm{sw}} = {} & c_{ij}^{\mathrm{sw,sect}} \sum_{t\in T}\sum_{ij\in E^{\mathrm{sw,sect}}} (\delta_{ij,t}^{\mathrm{sw,in}} + \delta_{ij,t}^{\mathrm{sw,de}}) + c_{ij}^{\mathrm{sw,feed}} \cdot \\ & \sum_{t\in T}\sum_{ij\in E^{\mathrm{sw,feed}}} (\delta_{ij,t}^{\mathrm{sw,in}} + \delta_{ij,t}^{\mathrm{sw,de}}) + c_{ij}^{\mathrm{sw,trans}} \sum_{t\in T}\sum_{ij\in E^{\mathrm{sw,trans}}} (\delta_{ij,t}^{\mathrm{sw,in}} + \delta_{ij,t}^{\mathrm{sw,de}}) + \\ & c_{ij}^{\mathrm{sw,sub}} \sum_{t\in T}\sum_{ij\in E^{\mathrm{sw,sub}}} (\delta_{ij,t}^{\mathrm{sw,in}} + \delta_{ij,t}^{\mathrm{sw,de}}) \end{aligned} \tag{4}$$

$$C^{\mathrm{lr}} = \sum_{t\in T}\Delta t \sum_{j\in B} c^{\mathrm{lr}} P_{j,t}^{\mathrm{lr}} \tag{5}$$

2) Load Balancing Index

The feeder load balancing index, transformer load balancing index, and substation balancing index are devised to express the global load balancing at different levels. More specifically, the feeder load balancing index represents the average value of mean square error for feeder power demand in all transformers while the transformer load balancing index represents that of mean square error for transformer power demand in all substations. As for substation load balancing, it is the mean square error of power load for all substations. Any one of them cannot represent the global load balancing degree well. In this way, the sum of three indexes should be optimized to improve the load balancing of the whole network, defined as the objective f_2.

$$\min f_2 = \sum_{t\in T}(B_t^{\mathrm{sub}} + B_t^{\mathrm{trans}} + B_t^{\mathrm{feed}}) \tag{6}$$

1) Substation load balancing index

$$\begin{cases} R_{j,t}^{\mathrm{sub}} = \dfrac{P_{j,t}^{\mathrm{sub}}}{P_j^{\mathrm{sub,max}}} & \forall t, \forall j \in B^{\mathrm{sub}} \\ R_t^{\mathrm{sub,avr}} = \dfrac{\sum_{j\in B^{\mathrm{sub}}} R_{j,t}^{\mathrm{sub}}}{N^{\mathrm{sub}}} & \forall t \\ B_t^{\mathrm{sub}} = \left\| R_{j,t}^{\mathrm{sub}} - R_t^{\mathrm{sub,avr}} \right\|_2 & \forall t \end{cases} \tag{7}$$

2) Transformer load balancing index

$$\begin{cases} R_{j,f,t}^{\text{trans}} = \dfrac{P_{j,f,t}^{\text{trans}}}{P_{j,f}^{\text{trans,max}}} & \forall t, \forall j \in B^{\text{sub}}, \forall f \in \gamma(j) \\ P_{j,f,t}^{\text{trans}} = \sum\limits_{k \in \alpha(j,f)} P_{jk,t} & \forall t, \forall j \in B^{\text{sub}}, \forall f \in \gamma(j) \\ B_{j,t}^{\text{trans}} = \left\| R_{j,f,t}^{\text{trans}} - R_{j,t}^{\text{trans,avr}} \right\|_2 & \forall t, \forall j \\ R_{j,t}^{\text{trans,avr}} = \dfrac{\sum\limits_{f \in \gamma(j)} R_{j,f,t}^{\text{trans}}}{N_j^{\text{trans}}} & \forall t, \forall j \\ B_t^{\text{trans}} = \dfrac{\sum\limits_{j \in B^{\text{sub}}} B_{j,t}^{\text{trans}}}{N^{\text{sub}}} & \forall t \end{cases} \tag{8}$$

3) Feeder load balancing index

$$\begin{cases} R_{jk,t}^{\text{feed}} = \dfrac{P_{jk,t}}{P_{jk}^{\max}} & \forall t, \forall j \in B^{\text{sub}}, \forall k \in \alpha(j,f) \\ R_{j,f,t}^{\text{feed,avr}} = \dfrac{\sum\limits_{k \in \alpha(j,f)} R_{jk,t}^{\text{feed}}}{N_{j,f}^{\text{feed}}} & \forall j, \forall f, \forall t \\ B_{j,f,t}^{\text{feed}} = \left\| R_{jk,t}^{\text{feed}} - R_{j,f,t}^{\text{feed,avr}} \right\|_2 & \forall j, \forall f, \forall t \\ B_t^{\text{feed}} = \sum\limits_{j \in B^{\text{sub}}} \sum\limits_{f \in \gamma(j)} \dfrac{B_{j,f,t}^{\text{feed}}}{N^{\text{trans}}} & \forall t \end{cases} \tag{9}$$

The expressions of mean square error are nonlinear equations as shown in (7)-(9), which can be relaxed into second-order cone expression (10) with a small relaxation gap in the programming simulation.

$$\begin{cases} \left\| R_{j,t}^{\text{sub}} - R_t^{\text{sub,avr}} \right\|_2 \le B_t^{\text{sub}} & \forall t \\ \left\| R_{j,f,t}^{\text{trans}} - R_{j,t}^{\text{trans,avr}} \right\|_2 \le B_{j,t}^{\text{trans}} & \forall t, \forall j \\ \left\| R_{jk,t}^{\text{feed}} - R_{j,f,t}^{\text{feed,avr}} \right\|_2 \le B_{j,f,t}^{\text{feed}} & \forall t, \forall j, \forall f \end{cases} \tag{10}$$

3) PVG Curtailment

The PVG curtailment is described as:

$$\min f_3 = A^{\text{PV}} \tag{11}$$

$$A^{\text{PV}} = \sum_{t \in T} \sum_{j \in B^{\text{PV}}} (P_{j,t}^{\text{PV,ava}} - P_{j,t}^{\text{PV}}) \tag{12}$$

C. Constraints

1) Distflow Model

The relaxed power flow model described in [19] is applied to transform the nonlinear constrains of power flow into second-order cone constraints. Additionally, the "big-M" -type constant M is used in (15). If $w_{ij,t}=1$, the switch branch ij is in operation, where the voltage relationship between the node i and node j is restricted by the branch flow and current. On the contrary, the constraint (15) always hold.

$$\sum_{k \in \alpha(j)} P_{jk,t} - \sum_{i \in \beta(j)} (P_{ij,t} - \hat{I}_{ij,t} r_{ij}) + g_j \hat{V}_{j,t} = P_{j,t} \quad \forall t, \forall j \in B \tag{13}$$

$$\sum_{k \in \alpha(j)} Q_{jk,t} - \sum_{i \in \beta(j)} (Q_{ij,t} - \hat{I}_{ij,t} x_{ij}) + b_j \hat{V}_{j,t} = Q_{j,t} \quad \forall t, \forall j \in B \tag{14}$$

$$\hat{V}_{j,t} + M(w_{ij,t} - 1) \le \hat{V}_{i,t} - 2(P_{ij,t} r_{ij} + Q_{ij,t} x_{ij}) + \hat{I}_{ij,t}(r_{ij}^2 + x_{ij}^2) \le \hat{V}_{j,t} + M(1 - w_{ij,t}) \quad \forall t, \forall ij \in E^{\text{sw}} \tag{15}$$

$$\hat{V}_{j,t} = \hat{V}_{i,t} - 2(P_{ij,t} r_{ij} + Q_{ij,t} x_{ij}) + \hat{I}_{ij,t}(r_{ij}^2 + x_{ij}^2) \quad \forall t, \forall ij \in E \backslash E^{\text{sw}} \tag{16}$$

$$\left\| \begin{matrix} 2P_{ij,t} \\ 2Q_{ij,t} \\ \hat{I}_{ij,t} - \hat{V}_{i,t} \end{matrix} \right\|_2 \le \hat{I}_{ij,t} + \hat{V}_{i,t} \quad \forall t, \forall ij \in E \tag{17}$$

$$P_{j,t} = P_{j,t}^{\text{sub}} + P_{j,t}^{\text{PV}} - P_{j,t}^{\text{l}} + P_{j,t}^{\text{lr}} \quad \forall t, \forall j \in B \tag{18}$$

$$Q_{j,t} = Q_{j,t}^{\text{sub}} - Q_{j,t}^{\text{l}} + Q_{j,t}^{\text{lr}} \quad \forall t, \forall j \in B \tag{19}$$

$$\hat{V}_{j,t} = V_{j,t}^2 \quad \forall t, \forall j \in B \tag{20}$$

$$\hat{I}_{ij,t} = I_{ij,t}^2 \quad \forall t, \forall ij \in E \tag{21}$$

2) Security Constraints

The security constraints are as follows.

$$\underline{I}_{ij}^2 \le \hat{I}_{ij,t} \le \bar{I}_{ij}^2 \quad \forall t, \forall ij \in E \backslash E^{\text{sw}} \tag{22}$$

$$w_{ij,t} \underline{I}_{ij}^2 \le \hat{I}_{ij,t} \le w_{ij,t} \bar{I}_{ij}^2 \quad \forall t, \forall ij \in E^{\text{sw}} \tag{23}$$

$$\underline{V}_j^2 \le \hat{V}_{j,t} \le \bar{V}_j^2 \quad \forall t, \forall j \in B \tag{24}$$

3) Network Reconfiguration

The dynamic reconfiguration with multi-level switching modes can be carried out by choosing different switch sets E^{sw}. Thus, the switching constraints can be expressed in a unified way.

1) Radiality

$$\sum_{ij \in E^{\text{sw}}} w_{ij,t} = B - N^{\text{sub}} - E^{\text{always}} \tag{25}$$

Equation (25) denotes that the number of connected branches is equal to the number of network nodes minus the number of substation nodes in a radial network.

2) Regulation limit

$$\delta_{ij,t}^{\text{sw,in}} + \delta_{ij,t}^{\text{sw,de}} \le 1 \quad \forall t, \forall ij \in E^{\text{sw}} \tag{26}$$

$$w_{ij,t} - w_{ij,t-1} = \delta_{ij,t}^{\text{sw,in}} - \delta_{ij,t}^{\text{sw,de}} \quad \forall t, \forall ij \in E^{\text{sw}} \tag{27}$$

$$\sum_{t \in T} (\delta_{ij,t}^{\text{sw,in}} + \delta_{ij,t}^{\text{sw,de}}) \le N_{ij}^{\text{sw,max}} \quad \forall ij \in E^{\text{sw}} \tag{28}$$

If $\delta_{ij,t}^{\text{sw,in}} = 1$, the status of the switch in branch ij changes from open to closed at time period t, and for $\delta_{ij,t}^{\text{sw,de}} = 1$, vice versa. Expression (26) denotes that the switch cannot be open or closed simultaneously. Note that $N_{ij}^{\text{sw,max}}$ can be set differently for three tie switches. $N_{ij}^{\text{sw,max}}$ can gradually decrease in the order of "feeder-transformer-substation" to roughly express the unwillingness of DSOs to frequently operate the switches located at the higher level, e.g., substation-level or transformer-level reconfiguration. In other words, the DSOs prefer to control the statuses of lower-level switches to reach a satisfactory balance performance.

3) Connectivity

The network radiality has been extensively studied in recent years, which aims to guarantee the topology radiality and connectivity after the network reconfiguration [22]-[24]. Equation (25) cannot totally ensure the network radiality, especially in the presence of PVG in UDN. Therefore, to avoid the existence of loops or islands, a small active load is added to PVG nodes and transition nodes (transition node is the node without power generation or demand) [22]. The additional auxiliary constraints (29)-(31) can guarantee the network connectivity. They are also associated with those switch variables in the above *Distflow* model.

$$\sum_{k\in\alpha(j)} P^{*}_{jk,t} - \sum_{i\in\beta(j)} P^{*}_{ij,t} = P^{*}_{j,t} = \varepsilon \quad \forall t, \forall j \in B \tag{29}$$

$$-w_{ij,t}P^{\max}_{ij} \le P^{*}_{ij,t} \le w_{ij,t}P^{\max}_{ij} \quad \forall t, \forall ij \in E^{\mathrm{sw}} \tag{30}$$

$$-P^{\max}_{ij} \le P^{*}_{ij,t} \le P^{\max}_{ij} \quad \forall t, \forall ij \in E\backslash E^{\mathrm{sw}} \tag{31}$$

4) Transformer Power Limit

The transformer power limit is as follows.

$$P^{\mathrm{trans,min}}_{j,f} \le P^{\mathrm{trans}}_{j,f,t} \le P^{\mathrm{trans,max}}_{j,f} \quad \forall t, \forall j \in B^{\mathrm{sub}}, \forall f \in \gamma(j) \tag{32}$$

$$\begin{cases} Q^{\mathrm{trans,min}}_{j,f} \le Q^{\mathrm{trans}}_{j,f,t} \le Q^{\mathrm{trans,max}}_{j,f} & \forall t, \forall j \in B^{\mathrm{sub}}, \forall f \in \gamma(j) \\ Q^{\mathrm{trans}}_{j,f,t} = \sum\limits_{k\in\alpha(j,f)} Q_{jk,t} & \forall t, \forall j \in B^{\mathrm{sub}}, \forall f \in \gamma(j) \end{cases} \tag{33}$$

5) PV Power Limit

The PV power limit is as follows.

$$0 \le P^{\mathrm{PV}}_{j,t} \le P^{\mathrm{PV,ava}}_{j,t} \tag{34}$$

6) Load Reduction Limit

The load reduction limit is as follows.

$$0 \le P^{\mathrm{lr}}_{j,t} \le \beta^{\mathrm{l}}_{j} P^{\mathrm{l}}_{j,t} \tag{35}$$

$$Q^{\mathrm{lr}}_{j,t} = P^{\mathrm{lr}}_{j,t} Q^{\mathrm{l}}_{j,t} / P^{\mathrm{l}}_{j,t} \tag{36}$$

IV. Stochastic Programming Model Based on Scenario Set

In this paper, the scenario set generated by the Monte Carlo method and *k*-means algorithm is used to address the uncertainties of PVGs and loads. Furthermore, the aforementioned multi-objective function is normalized into a single objective function by $\bar{\lambda}_1$, $\bar{\lambda}_2$, $\bar{\lambda}_3$. Then the stochastic programming model can be expressed in the following compact matrix form.

$$\min\left(\bar{\lambda}_1 f_1 + \bar{\lambda}_2 f_2 + \bar{\lambda}_3 f_3\right) \tag{37}$$

$$f_1 = C^{\mathrm{sw}} + \sum_{s\in N_s} f_s \left(C^{\mathrm{loss}}_{s} + C^{\mathrm{sub}}_{s}\right) \tag{38}$$

$$f_2 = \sum_{s\in N_s} f_s \sum_{t\in T} \left(B^{\mathrm{sub}}_{s,t} + B^{\mathrm{trans}}_{s,t} + B^{\mathrm{feed}}_{s,t}\right) \tag{39}$$

$$f_3 = \sum_{s\in N_s} f_s A^{\mathrm{PV}}_{s} \tag{40}$$

s.t.

$$\boldsymbol{A}\boldsymbol{x} \le \boldsymbol{b} \tag{41}$$

$$\boldsymbol{C}\boldsymbol{x} = \boldsymbol{d} \tag{42}$$

$$\boldsymbol{G}\boldsymbol{x} + \boldsymbol{H}\boldsymbol{y}_s = \boldsymbol{k} \tag{43}$$

$$\left\| \boldsymbol{L}\boldsymbol{y}_s \right\|_2 \le \boldsymbol{M}^{\mathrm{T}} \boldsymbol{y}_s \tag{44}$$

$$\boldsymbol{J}\boldsymbol{y}_s \le \boldsymbol{w} \tag{45}$$

$$\boldsymbol{R}\boldsymbol{y}_s \le \boldsymbol{\xi}_s \tag{46}$$

The first-stage decision variables are related to the switches and power flow in the connectivity constraints, while the PV power, load reduction, and transformer power are intended for the second-stage decision variables.

The objective function (37) is determined by both the first-stage and second-stage decision variables. Equations (41) and (42) denote the network reconfiguration constrains. The first-stage and second-stage decision variables are coupled by (43). Equation (44) denotes the second-order cone constraints, including the relaxed real power flow and load balancing index. The inequality constraints of the second-stage variables in each scenario are shown in (45). Lastly, (46) denotes the PV power limit.

V. Solution Methodology

A. Fuzzy C-means Clustering-based Time Period Division

The dynamic reconfiguration can be effectively conducted due to the unbalanced spatial-temporal distribution of power generations and demands. However, the dynamic reconfiguration in the whole time horizon would lead to a high computational burden due to a large number of binary variables. Therefore, we decrease the calculation dimension based on the time division. Each division (including several continuous time periods) is assigned to only one network topology when solving the reconfiguration model. In this paper, we adopt FCM [20] to divide the time periods. FCM performs the division (clustering) by a loss function based on a fuzzy membership matrix. Especially, it assigns the membership degrees of given data to all cluster centers in the interval [0,1], which breaks the single membership relationship of hard clustering. Hereby, the points belonging to a cluster can achieve the smallest difference, which are opposite for different clusters.

The clustering programming model of FCM can be formulated as:

$$\min J(\boldsymbol{X},\boldsymbol{U},\boldsymbol{V}) = \sum_{c\in C}\sum_{t\in T} u^{b}_{c,t} d^{2}_{c,t} = \sum_{c\in C}\sum_{t\in T} u^{b}_{c,t} \left\| \boldsymbol{X}_t - \boldsymbol{V}_c \right\|^2 \quad b \ge 1 \tag{47}$$

$$\begin{cases} \sum\limits_{c\in C} u_{c,t} = 1 & \forall t \\ 0 \le u_{c,t} \le 1 & \forall c, \forall t \end{cases} \tag{48}$$

As a weighted index number, b is usually equal to 2 to ensure the astringency. In addition, (48) indicates that the sum of membership degrees of $\boldsymbol{X}_t$ to all clusters is equal to 1, which is a typical feature of FCM. The optimal $\boldsymbol{U}_{C\times T}$ and $\boldsymbol{V}$ for (47) and (48) can be obtained by (49) and (50), respectively.

$$u_{c,t} = \left(\sum_{m\in C} \left(\frac{d_{c,t}}{d_{m,t}} \right)^{\frac{2}{b-1}} \right)^{-1} \tag{49}$$

$$\boldsymbol{V}_c = \frac{\sum\limits_{t\in T} u^{b}_{c,t} \boldsymbol{X}_t}{\sum\limits_{t\in T} u^{b}_{c,t}} \tag{50}$$

The overall clustering procedure can be summarized as:

Step 1: initialize the number of clusters C, $\boldsymbol{U}_{C\times T}$, and the tolerance ε. $k = 1$.

Step 2: calculate $\boldsymbol{V}^k$ according to (50).

Step 3: update $\boldsymbol{U}^k$ according to (49).

Step 4: if $\left\| \boldsymbol{U}^{k+1}_{C\times T} - \boldsymbol{U}^{k}_{C\times T} \right\| < \varepsilon$, return $\boldsymbol{V}^k$ and $\boldsymbol{U}^k$. Otherwise, update $k = k+1$ and go to *Step 2*.

Step 5: based on the clustering result, the isolated points can be further classified into the adjacent cluster with a higher membership degree.

By using FCM, the whole time periods can be divided into M clusters, which means the time dimension of dynamic reconfiguration is reduced from T to M. In the FCM process,

setting an optimal cluster number is significant. The regulation limit is used to avoid frequently changing the switch state, as shown in the previous section. It is noted that the optimal number of clusters is not required in the above FCM. The stochastic programming model proposed in Section IV needs to be modified slightly, where the dimension of switch variables decreases from T to M. It can be realized by the cluster-time periods incidence matrix $\boldsymbol{RM}$. If the time period j belongs to reconfiguration time period i, $rm_{ij}=1$,

$$\boldsymbol{RM}=\begin{bmatrix} rm_{11} & rm_{12} & \cdots & rm_{1T} \\ rm_{21} & rm_{22} & \cdots & rm_{2T} \\ \vdots & \vdots & & \vdots \\ rm_{M1} & rm_{M2} & \cdots & rm_{MT} \end{bmatrix} \tag{51}$$

B. BPSO and Cplex-based Combinational Method to Solve Proposed Model

The formulated MISOCP model is still challenging to solve when applied in large-scale systems because of the numerous binary variables. Thus, a combinational way based on the modified BPSO and commercial solver Cplex is used in this subsection. The BPSO takes the switch states as random swarms and embeds Cplex to solve the SOCP model corresponding to various particles. Meanwhile, the fitness values received from Cplex computation would be the key point to the evolution of the swarm in the BPSO iterations. The overall procedure is shown in Fig. 5.

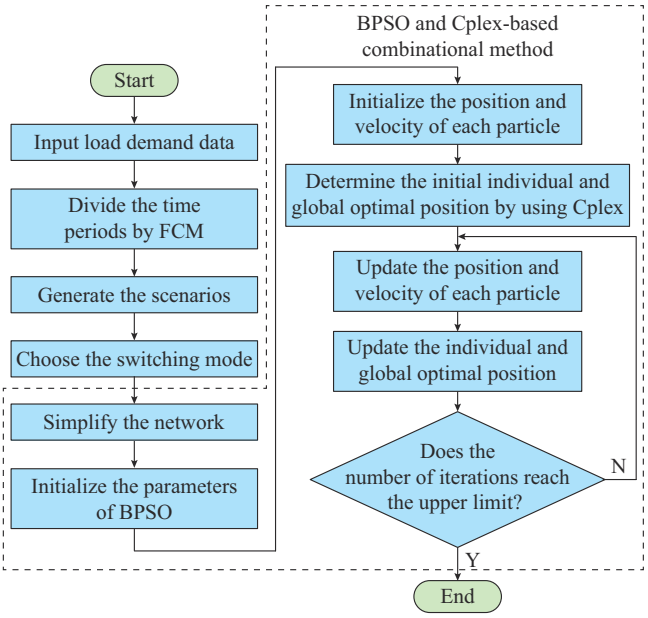

Fig. 5. Flowchart of solution algorithm.

The BPSO was initially proposed by Eberhart and Kennedy in 1997 [21]. However, the network topology may be infeasible when directly coding each switch state as 0-1. Obviously, the closing of the tie switch must be accompanied by the opening of the sectionalizing switch to satisfy the network radiality. Therefore, an improved coding rule based on the loop is adopted so as to ensure the topology feasibility (radiality) when generating the initial particles and updating particles.

Significantly, the initial particle implementation is demonstrated in the following steps.

Step 1: particle coding. The initial velocities of particles are set randomly in a limited range. The position of the i^{th} particle can be expressed as $\boldsymbol{x}_i=(\boldsymbol{x}_{i1},\boldsymbol{x}_{i2},...,\boldsymbol{x}_{im},...,\boldsymbol{x}_{iM})$, where $\boldsymbol{x}_{im}=(x_{im1},x_{im2},...,x_{imN^{\text{swr}}})$. Note that we code the position of the particle in each time period in turn to guarantee the radiality and connectivity of network topology at any time. Moreover, *Step 1* and the following *Steps 2-4* only present the coding procedure in each time period. Randomly assign $\boldsymbol{x}_{im}=(x_{im1},x_{im2},...,x_{imN^{\text{swr}}})$ and ensure that the number of "0" in each loop is equal to 1.

Step 2: radiality check. In terms of *Step 1*, the loops or islands may exist if the branches corresponding to "0" in multiple loops are in the same branch. Therefore, the number of loops is forced to be the number of open switches, which could be given by decoding the particle via the switch-loop switch incidence matrix $\boldsymbol{P}$. If the number of open switches in *Step 1* satisfies this condition, go to the next step. Otherwise, go to *Step 1*.

$$\boldsymbol{P}=\begin{bmatrix} p_{11} & p_{12} & \cdots & p_{1q} & \cdots & p_{1N^{\text{swr}}} \\ p_{21} & p_{22} & \cdots & p_{2q} & \cdots & p_{2N^{\text{swr}}} \\ \vdots & \vdots & & \vdots & & \vdots \\ p_{N^{\text{sw}}1} & p_{N^{\text{sw}}2} & \cdots & p_{N^{\text{sw}}q} & \cdots & p_{N^{\text{sw}}N^{\text{swr}}} \end{bmatrix} \tag{52}$$

If $p_{iq}=1$, it means that the switch i is deployed on the branch q. In addition, only one element in the same column of matrix $\boldsymbol{P}$ can be 1, while more than one element in the same row can be equal to 1, which indicates that the switch branch is the public branch contained in multiple loops.

Step 3: connectivity check. The node adjacency matrix is calculated by node-branch incidence matrix and decoded switch state vector. Then, the Laplacian matrix for connectivity discrimination is formed. If the particle satisfies network topology constraints, go to the next step. Otherwise, go to *Step 1*.

Step 4: regulation limit check. If the switch state vector from the decoding particle violates (28), it will stop. Otherwise, go to *Step 1*.

It is ensured that the initial particles obtained by the above steps are feasible solutions. The particle updating is similar to the initial particle implementation except *Step 1*. Specifically, the velocity of the particle is updated by (53). The sigmoid function (54) is used to calculate the probability of "0" in each dimension of the particle position. Furthermore, the roulette algorithm is used to select the "0" dimension in each loop as follows.

1) Calculate the selection probability of "0" in each dimension of each loop by $S(\boldsymbol{v}_{im}^{n+1})$.

2) Calculate the cumulative probability.

3) Compare the random number in the interval [0,1] and the cumulative probability. The "0" in each loop will be decided.

$$\boldsymbol{v}_{im}^{n+1}=\boldsymbol{v}_{im}^{n}+c_1r_1(\boldsymbol{p}_{im}^{n}-\boldsymbol{x}_{im}^{n})+c_2r_2(\boldsymbol{p}_{gm}^{n}-\boldsymbol{x}_{im}^{n}) \tag{53}$$

$$S(\boldsymbol{v}_{im}^{n+1})=1-1/(1+\exp(-\boldsymbol{v}_{im}^{n+1})) \tag{54}$$

Then, the updated particle position can meet the requirement that the number of "0" in each loop is equal to 1. Therefore, the updated particles will be feasible after checking the above *Steps 2-4*.

VI. Case Studies

The modified 148-node system and 297-node system are used to validate the proposed method in this paper. All the computations are carried out on a 2.9 GHz personal computer with 8 GB RAM, and the proposed method is programmed in MATLAB 2016a.

A. Validation of Proposed Method in 148-node System

1) System Configuration

As shown in Fig. 6, the test system consists of two substations, four transformers, and eight feeders. The spatial-temporal distribution of power generations and demands in practical UDN is unbalanced. For simplicity, it is assumed that PVGs are only connected to one feeder of each transformer. Moreover, the forecasted power outputs of PVGs are assumed to be the same in each node. Load forecasting data (active power) in eight feeders are shown in Fig. 7. The number of sectionalizing switches, feeder tie switches, transformer tie switches and substation tie switches are 13, 7, 3, and 2, respectively while the switching costs of these switches are \$50, \$50, \$100, and \$150, respectively. And the maximum regulation numbers in the whole time horizon are 4, 4, 3, and 2, respectively. The inertia weight of the BPSO algorithm is updated adaptively and is restricted within [0.4, 0.9]. The learning factors c_1 and c_2 are both 2. The size of the swarm is 30.

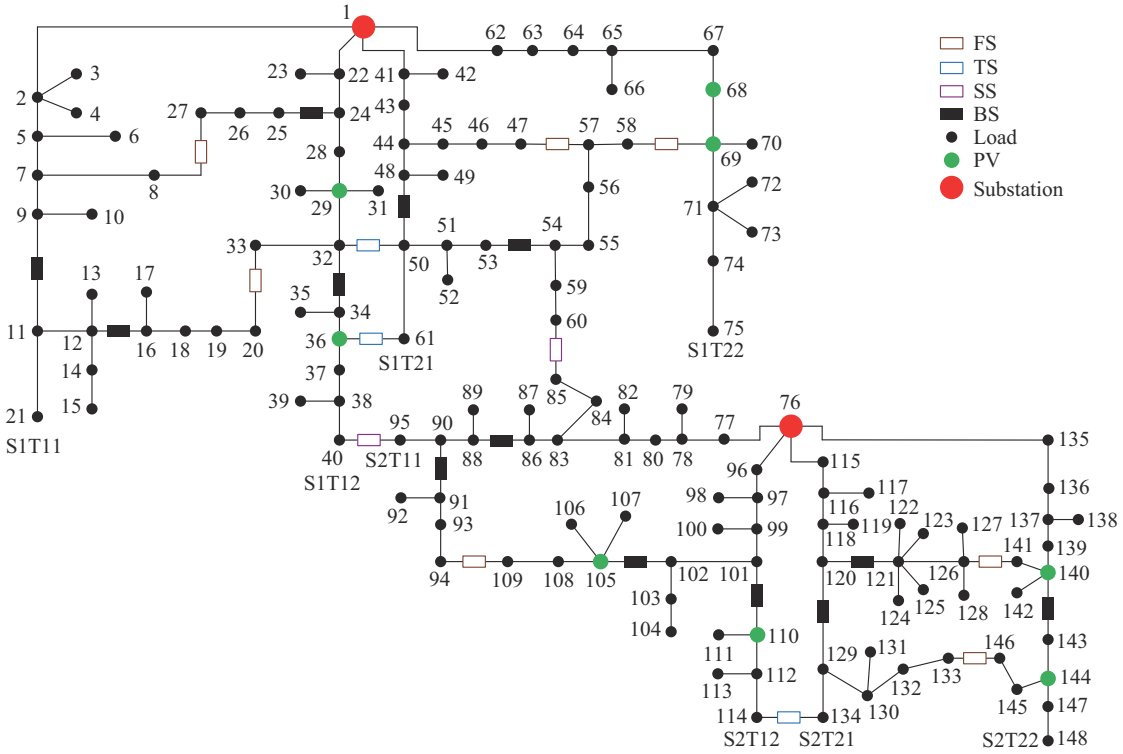

Fig. 6. Topology of 148-node system.

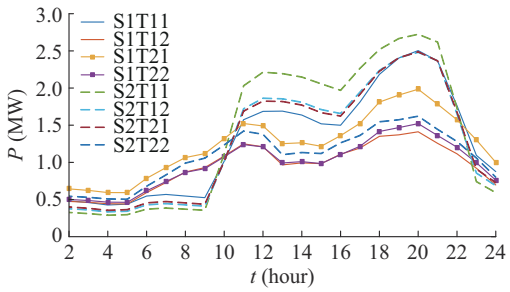

Fig. 7. Load forecasting data (active power) in eight feeders.

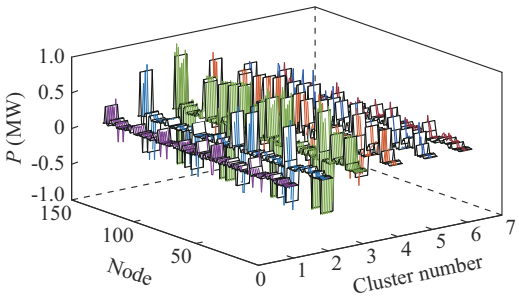

Fig. 8. Clustering results of basic scenario.

Taking the basic scenario as an example, the schedule horizon is divided into six clusters by the FCM. Specifically, the time division includes time period 1-6, time period 7-9, time period 10-17, time period 18-20, time period 21-22, and time period 23-24. As shown in Fig. 8, the curves on the strip (the cluster center) represent the spatial distribution of the load demands during different periods belonging to this cluster.

2) Analysis of Deterministic Dynamic Reconfiguration with Multi-level Switching Modes

Considering the unbalanced distribution of load demands in the UDN, two case sets with different PVG penetration and load rates are devised in this part to explore the incremental benefits of dynamic reconfiguration among multi-level switching modes. Then, an ideal switching mode can be

recommended for DSOs according to the results.

1) Analysis of multi-level switching modes with different PVG penetration

The capacities of PVGs in feeders S1T12, S1T22, S2T12, and S2T22 are adjusted to generate different spatial-temporal distribution of load demands. As reported in Table II, eight cases with different PV penetration are set up for the dynamic reconfiguration. Note that the PVG curtailment and overall objective would be emphatically analyzed.

TABLE II
CASES FOR DIFFERENT PVG PENETRATIONS

Case	Capacity of PVG (MW)	Penetration (%)
1	S1T12: 2, S2T12: 0.5, S1T22/S2T22: 1	26.88
2	S2T12: 2.5, S1T12/S1T22/S2T22: 1	32.85
3	S1T12/S1T22/S2T12/S2T22: 1.5	35.84
4	S1T12: 3, S1T22: 2, S2T12: 0.5, S2T22: 1	38.82
5	S1T12/S2T12: 2.4, S1T22/S2T22: 1.5	46.59
6	S1T12/S1T22/S2T12/S2T22: 2	47.78
7	S1T12/S2T12: 2.7, S1T22/S2T22: 1.5	50.17
8	S1T12/S2T12: 3, S1T22/S2T22: 1.5	53.76

When the PVG outputs in several feeders are too large to be fully absorbed, network reconfiguration is needed to improve the power flow distribution for increasing the PVG consumption. As shown in Fig. 9, for different cases, PVG curtailment reduction is incurred by adopting three switching modes.

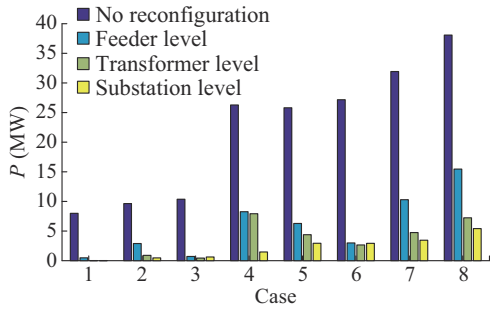

Fig. 9. PVG curtailments under original network topology and three switching modes.

In most cases, the PVG curtailment gradually decreases when changing the switching mode from feeder level to substation level. In other words, the reduction performance of PVG curtailment is optimal when conducting substation-level reconfiguration because all the switches are involved at the same time. Moreover, it can be observed that the PVG curtailment depends on not only the PVG penetration but also the spatial distribution of load demands. For instance, the PVG curtailments in cases 5 and 6 are different.

In cases 1, 3, and 6, the PVG curtailment reductions at the transformer level and substation level are not remarkable, especially when the PVG power is almost fully absorbed by the feeder-level reconfiguration. Similarly, from cases 2, 5, 7 and 8, it is found that the transformer-level reconfiguration can effectively reduce the PVG curtailment, and thus substation-level reconfiguration is unnecessary. Nevertheless, in case 4, the substation-level reconfiguration has a great effect on the PVG curtailment. Thus, the PVG utilization difference resulted from the feeder level to the substation-level dynamic reconfiguration in each case is not the same.

From the total objective and load balancing index in multiple switching modes illustrated in Fig. 10, the following observations can be made. Firstly, no or only small incremental benefit is obtained when changing the reconfiguration from feeder level to substation level in some cases. This reflects that the transfer capacity of higher-level (substation-level or transformer-level) reconfiguration is insufficient. In such cases, the lower-level switching mode outperforms the higher-level one when DSOs give preference to the lower-level switches. Secondly, there is no monotonic relationship between the load balancing index and the multi-level switching modes. The load balancing preference may be sacrificed while ensuring the PVG curtailment reduction. It also implies that the network reconfiguration heavily relies on certain transferable branches, and the sectionalizing switches may have been unreasonably deployed.

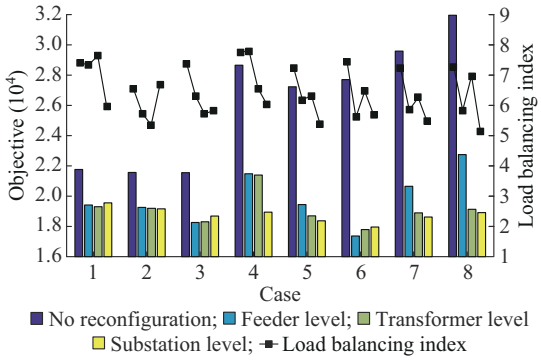

Fig. 10. Total objective and load balancing index under original network topology and dynamic reconfiguration with multi-level switching modes.

Meanwhile, it is important to highlight that the three switching modes of dynamic reconfiguration have dramatically reduced the PVG curtailment as well as the total objective compared with the original network topology. However, the incremental benefits from feeder level to substation level are not guaranteed to be growing in certain cases. Therefore, an appropriate switching mode should be chosen according to the total objective result in the three reconfiguration modes so as to prevent the low incremental benefit when applying the higher-level switching mode. According to the optimization results of the total objective, the feeder-level reconfiguration should be selected in cases 1, 2, 3, and 6, while the transformer-level reconfiguration is better in cases 5, 7, and 8. The substation level would be a better choice for case 4.

2) Analysis on multi-level switching modes under different load rates

Similarly, we adjust the load rate of some feeders based on the basic data shown in Fig. 7. Then eight cases reported in Table III are intended for the unbalanced spatial-temporal distribution of load demands. This part mainly focuses on the influence of multi-level switching modes under different load rates. Thus, the PVG penetration in those eight cases is

set unchanged and is at a low level. According to the numerical result, there is no PVG curtailment in those cases when performing the switching mode at any level.

TABLE III
CASES FOR DIFFERENT LOAD RATES

Case	Capacity of load rate (MW)	Capacity-load ratio
1	S1T11/S1T21: 1.4	1.34
2	S2T11/S2T12: 1.28	1.37
3	S2T11/S2T12: 1.35	1.34
4	S1T11/S1T21/S2T11/S2T21: 1.25	1.29
5	S1T11/S1T21/S2T11/S2T21: 1.28	1.27
6	S1T11/S1T21/S2T11/S2T21: 1.33	1.24
7	S2T11/S2T12/S2T21/S2T22: 1.22	1.33
8	Whole network: 1.3	1.14

As shown in Fig. 11, the load shedding cost is high in all the cases due to the transmission power limit of the feeders and transformers when no reconfiguration is applied and the load demand is high. However, the application of dynamic reconfiguration can effectively alleviate this problem. It can be seen that the load shedding cost gradually decreases in each case and even drops to 0 in some cases when applying the reconfiguration from feeder level to substation level.

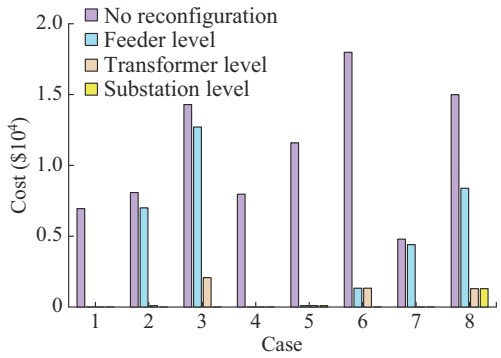

Fig. 11. Load shedding cost under original network topology and multi-level switching modes.

Specifically, the impacts of multi-level switching modes on the load shedding cost in these cases are analyzed in detail. In cases 2 and 3, the feeder-level reconfiguration has a negligible effect on load shedding. It shows that both feeders linked to transformer S2T1 have a high load demand concurrently, and thus the feeder-transfer cannot guarantee the reliable power supply. In other words, the high-level transfer is necessary. Moreover, comparing case 2 with case 3, it can be seen that the transformer-level switching mode can ensure no load shedding when the load rate in S2T1 is less than 1.28 times of the basic data. Otherwise, the substation-level switching is required. When the unbalance degree of load demand distribution increases globally such as cases 4-6, the feeder-level switching would be unable to guarantee the reliability of power supply if the load rate reaches 1.28 times of the basic data. In addition, the comparison between case 2 and case 5 shows that the load demand in S2T11 is higher than that in S2T12, and the sectionalizing switches of S2T11 are not reasonably deployed because the transferable power is either too small or too large. As far as the growth of load rate in substation 2 is concerned, the transformer-level reconfiguration is enough to ensure no load shedding if the load rate is less than 1.22 times of the basic data. Furthermore, the transfer capabilities of all three switching modes would be weakened with the increase of global load power. As shown in case 8, the performance by the substation-level model is almost the same as that by the transformer-level one.

The total objective and load balancing index with multiple modes under different load rates are illustrated in Fig. 12. Similar to the results under different levels of PVG penetration, there is no monotonic relationship between the load balancing index and the multi-level switching modes. The optimization of the total objective is expected. Specially, the dynamic reconfiguration with multi-level switching modes has significantly reduced the load shedding cost and the total objective value. But the incremental benefits from feeder level to substation level may vary in different cases. In addition, the total objective by using some higher-level mode may be higher than that by using a lower-level mode in some cases. Such phenomenon is related to the limitation of BPSO in the combinational method. In another way, it also illustrates that the incremental benefit from the lower-level mode to the higher-level mode would not be significant. According to the total objective value, the feeder-level switching mode is a better choice in cases 1, 4, 5, and 6. The transformer-level switching mode should be selected in cases 2, 7, and 8, while the substation-level mode would be the best for case 3.

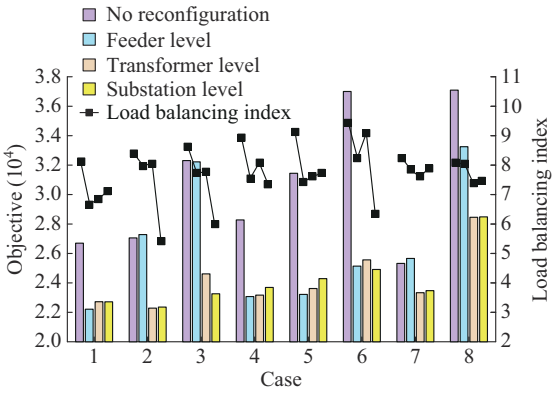

Fig. 12. Total objective and load balancing index under original network topology and multi-level switching modes.

3) Comparison of Stochastic Programming Model with Deterministic Model

Using case 6 in Table II as an example, 1000000 scenarios are randomly generated to compare the reconfiguration schemes between stochastic programming and deterministic model. The test results are presented in Table IV. It can be observed that both the maximum objective value and the average objective value of the stochastic programming model are smaller than those of the deterministic model, which indicates that the stochastic programming has a better performance in dealing with the uncertainties.

TABLE IV
COMPARISON OF TEST RESULTS BETWEEN STOCHASTIC PROGRAMMING AND DETERMINISTIC MODEL

Type	The maximum objective value	Average objective value
Stochastic programing	20840.6140	18723.6969
Deterministic model	21038.7156	18796.1879

4) SOCR Exactness Analysis

The branch power and current must be 0 when the status of a switch branch changes from closed to open. The feeder load rate and feeder load balancing index of a transformer may be close to 0 during some time periods due to the high PVG penetration. Note that both situations would lead to serious distortion of the relative relaxation gap. Consequently, we define the absolute relaxation gaps to check the exactness of (10) and (17) as:

$$\begin{cases} \Delta_t^{\text{sub, diff}} = \left| \left\| R_{j,t}^{\text{sub}} - R_t^{\text{sub, avr}} \right\|_2 - B_t^{\text{sub}} \right| \\ \Delta_{j,t}^{\text{trans, diff}} = \left| \left\| R_{j,f,t}^{\text{trans}} - R_{j,t}^{\text{trans, avr}} \right\|_2 - B_{j,t}^{\text{trans}} \right| \\ \Delta_{j,f,t}^{\text{feed, diff}} = \left| \left\| R_{jk,t}^{\text{feed}} - R_{j,f,t}^{\text{feed, avr}} \right\|_2 - B_{j,f,t}^{\text{feed}} \right| \end{cases} \tag{55}$$

$$\Delta_{ij,t}^{\text{diff}} = \left| (P_{ij,t}^2 + Q_{ij,t}^2)/V_{i,t}^{\wedge} - I_{ij,t}^{\wedge} \right| \quad \forall t, \forall ij \in E \tag{56}$$

For case 6 in Table II, the relaxation gaps of the three balancing indexes and branch current are shown in Figs. 13 and 14, respectively. It can be observed that the order of magnitude of the relaxation gaps is around 10^{-10} and 10^{-7}, which indicates that the second-order cone relaxation adopted in this paper is sufficiently accurate.

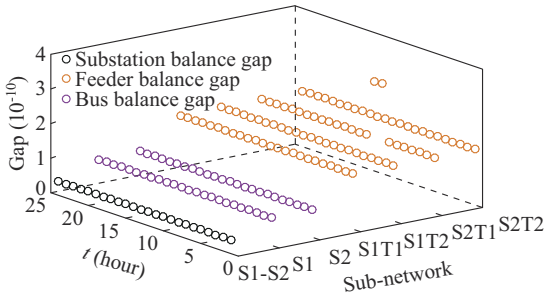

Fig. 13. Gap scatter for load balancing index.

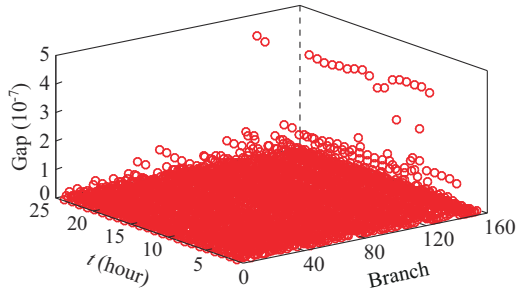

Fig. 14. Gap scatter for current.

5) Comparison of Different Solution Methods

Different solution methods are used to solve the MISOCP model established in the Section IV. The comparation of processing time is shown in Table V, where we can find that it is infeasible to solve the problem by Cplex due to the numerous binary variables.

Also, the updated individuals after the crossover and mutation of genetic algorithm (GA) are usually infeasible, which decelerate the optimization. As expected, the processing time of the proposed method is shorter than that of GA.

TABLE V
COMPARISON OF PROCESSING TIME OF DIFFERENT SOLUTION METHODS

Method	Processing time (hour)
Cplex	Infeasible
Combinational method (BPSO-Cplex)	11.82
GA	20.49

6) Comparison of Different Switching costs

Different switching costs are selected to compare the total objective obtained by multi-level switching modes. In the above numerical analysis, the switching costs of feeder tie switch, transformer tie switch and substation tie switch are set to be \$50, \$100, and \$150, respectively. We make this objective as cost 2 in this part. In addition, other two tests are included, whose objectives are named as cost 1 (\$50, \$150, and \$250) and cost 3 (\$50, \$75, and \$100). For cases 5, 7, and 8 in Table II, the total objectives obtained by selecting different switching costs in multi-level switching modes are shown in Fig. 15. It indicates that the incremental benefits from feeder-level switching mode to substation-level switching mode would decrease as the switching cost of high-level switches increases. In this way, the willingness to choose low-level reconfiguration would be stronger due to the high switching cost of high-level switches.

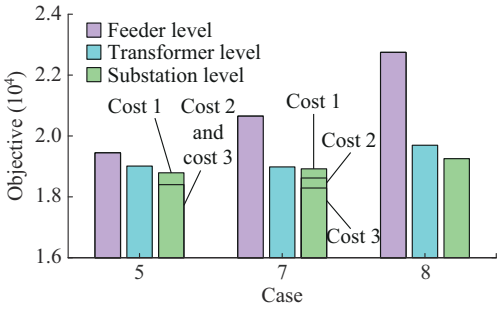

Fig. 15. Total objective obtained by using different switching costs in multi-level switching modes.

B. Validation of Proposed Method in 297-node System

A practical system which includes 297 nodes, two substations, four transformers, and eight feeders is applied to test the proposed method. The topology of this system is depicted in Fig. 16. The numbers of sectionalizing switches, feeder tie switches, transformer tie switches, and substation tie switches are 19, 7, 3, and 2, respectively. The forecasted loads in eight feeders are shown in Fig. 17. Some other parameters are also the same as those described in the 148-node system.

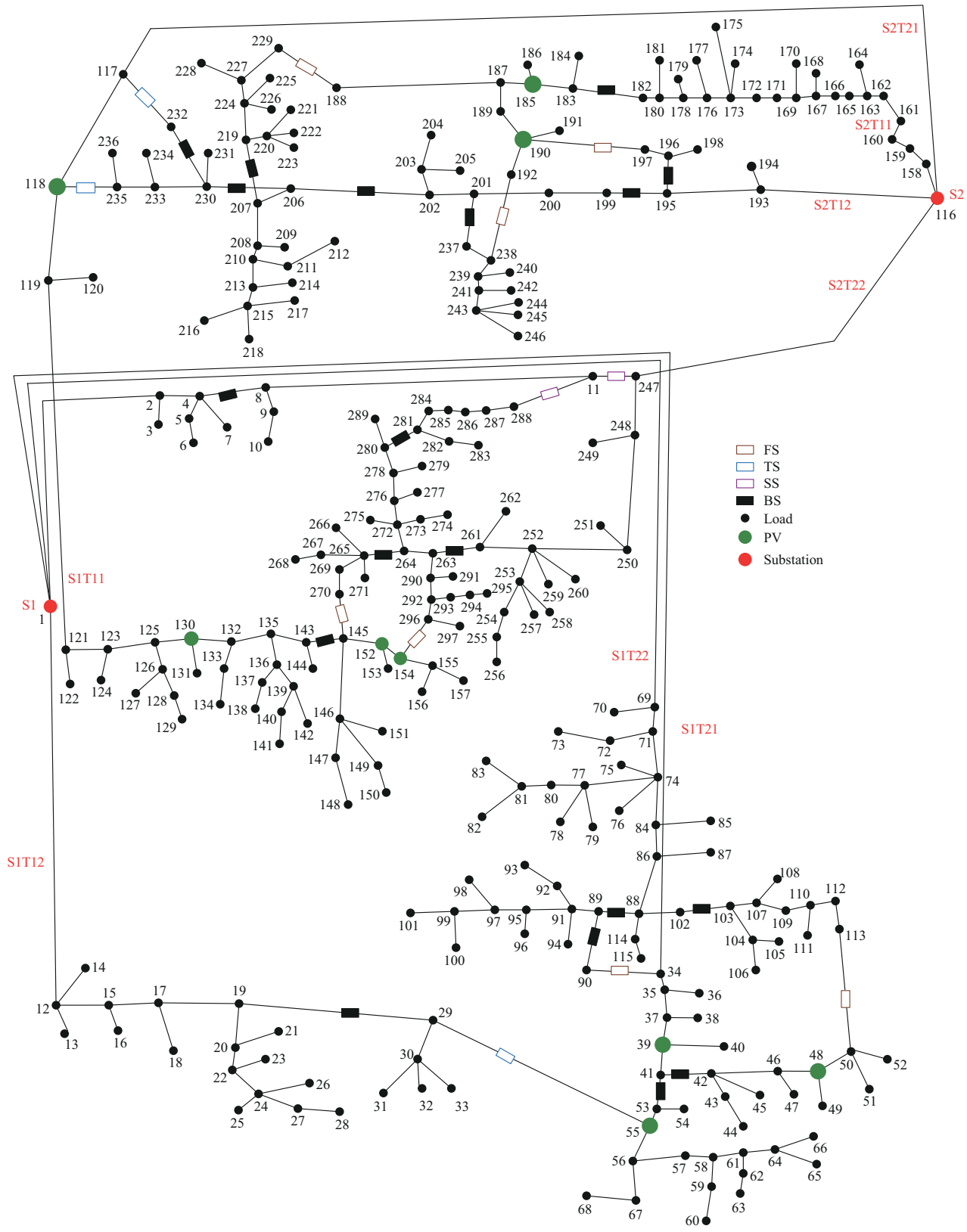

Fig. 16. Topology of 297-node system.

Similarly, the capacities of PVGs in feeders S1T21, S2T11, and S2T21 are adjusted in various ways to change the distribution of load demand. Then, four cases reported in Table VI are selected to explore the increasing benefits from feeder-level reconfiguration to substation-level reconfiguration. The test results including PVG curtailment and total objective are shown in Fig. 18.

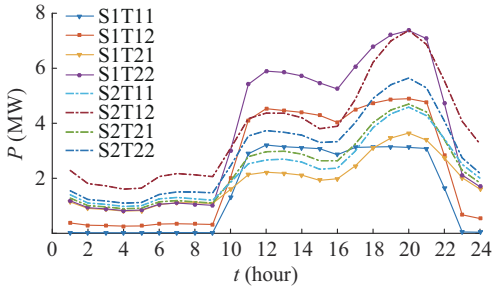

Fig. 17. Load forecast data (active power) of eight feeders in 297-node system.

TABLE VI
CASES FOR DIFFERENT PVG PENETRATIONS

Case	Capacity of PVG (MW)	Penetration (%)
1	S1T21: 3, S2T11: 2, S2T21: 4	21.77
2	S1T21: 3, S2T11: 2, S2T21: 6	26.60
3	S1T21: 3, S2T11: 3, S2T21: 4	24.18
4	S1T21: 4.5, S2T11: 2, S2T21: 4	25.39

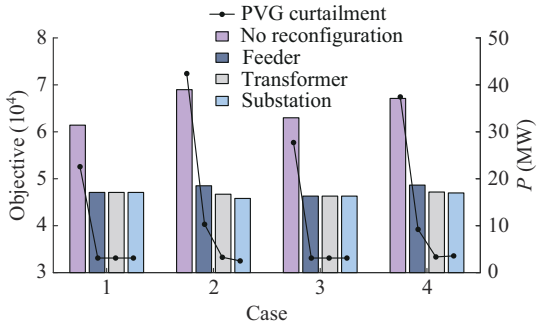

Fig. 18. Total objective and PVG curtailment under original network topology and multi-level switching modes.

The serious PVG curtailment under the original network topology is caused by the unbalanced distribution of load demands. The power flow regulation performed by multi-level switching modes would improve this situation. However, the increasing benefits brought by the higher-level reconfiguration may be so slight. As shown in Fig. 18, the small increasing benefit is obtained from feeder level to transformer level in case 2 and case 4 while there is no benefit when changing from feeder level to substation level in case 1 and case 3. According to the total objective, the feeder-level reconfiguration should be selected in cases 1-4.

VII. CONCLUSION

This paper proposes a dynamic reconfiguration model for multi-level switching modes to minimize the operation cost, load imbalance and PVG curtailment. The multi-level switching modes are characterized according to the participation of different tie switches. Case studies are performed to show the effectiveness of the proposed model. The conclusions are summarized as follows.

1) The incremental benefits of multi-level switching modes may vary with different PVG penetrations and load demands in the UDN. To avoid the large-scale power flow regulations, a suitable switching mode should be optimized to support the generation-demand balance. Furthermore, if the alleviation of PVG curtailment or load shedding is achieved with the sacrifice of load balancing, it implies that the capability in transferring power flow is insufficient.

2) Compared with the deterministic method, the stochastic model demonstrates better performance in handling the uncertainties of PVGs and loads and improving the optimization results for dynamic reconfiguration.

3) The second-order cone relaxation of load balancing index and power flow in this paper are exact.

4) The incremental benefits from feeder level to substation level would decrease as the switching cost of high-level switches increases.

REFERENCES

[1] N. C. Koutsoukis, D. O. Siagkas, P. S. Georgilakis *et al*., "Online reconfiguration of active distribution networks for maximum integration of distributed generation," *IEEE Transactions on Automation Science and Engineering*, vol. 14, no. 2, pp. 437-448, Apr. 2017.
[2] F. Capitanescu, L. F. Ochoa, H. Margossian *et al*., "Assessing the potential of network reconfiguration to improve distributed generation hosting capacity in active distribution systems," *IEEE Transactions on Power Systems*, vol. 30, no. 1, pp. 346-356, Jan. 2015.
[3] C. Lee, C. Liu, S. Mehrotra *et al*., "Robust distribution network reconfiguration," *IEEE Transactions on Smart Grid*, vol. 6, no. 2, pp. 836-842, Mar. 2015.
[4] A. Azizivahed, A. Arefi, S. Ghavidel *et al*., "Energy management strategy in dynamic distribution network reconfiguration considering renewable energy resources and storage," *IEEE Transactions on Sustainable Energy*, vol. 11, no. 2, pp. 662-673, Apr. 2020.
[5] M. A. Heidari, "Optimal network reconfiguration in distribution system for loss reduction and voltage-profile improvement using hybrid algorithm of PSO and ACO," *CIRED–Open Access Proceedings Journal*, vol. 2017, no. 1, pp. 2458-2461, Jun. 2017.
[6] M. A. Kashem, V. Ganapathy, and G. B. Jasmon, "Network reconfiguration for load balancing in distribution networks," *IEE Proceedings–Generation, Transmission and Distribution*, vol. 146, no. 6, pp. 563-567, Nov. 1999.
[7] S. R. Tuladhar, J. G. Singh, and W. Ongsakul, "Multi-objective approach for distribution network reconfiguration with optimal DG power factor using NSPSO," *IET Generation, Transmission & Distribution*, vol. 10, no. 12, pp. 2842-2851, May 2016.
[8] J. Wang, W. Wang, Z. Yuan *et al*., "A chaos disturbed beetle antennae search algorithm for a multi-objective distribution network reconfiguration considering the variation of load and DG," *IEEE Access*, vol. 8, pp. 97392-97407, Jun. 2020.
[9] Y. Song, Y. Zheng, T. Liu *et al*., "A new formulation of distribution network reconfiguration for reducing the voltage volatility induced by distributed generation," *IEEE Transactions on Power Systems*, vol. 35, no. 1, pp. 496-507, Jan. 2020.
[10] H. Wu, P. Dong, and M. Liu, "Distribution network reconfiguration for loss reduction and voltage stability with random fuzzy uncertainties of renewable energy generation and load," *IEEE Transactions on Industrial Informatics*, vol. 16, no. 9, pp. 5655-5666, Sept. 2020.
[11] C. Wang, S. Lei, P. Ju *et al*., "MDP-based distribution network reconfiguration with renewable distributed generation: approximate dynamic programming approach," *IEEE Transactions on Smart Grid*, vol. 11, no. 4, pp. 3620-3631, Jul. 2020.
[12] S. Lei, Y. Hou, F. Qiu *et al*., "Identification of critical switches for integrating renewable distributed generation by dynamic network reconfiguration," *IEEE Transactions on Sustainable Energy*, vol. 9, no. 1, pp. 420-432, Jan. 2018.
[13] H. Ahmadi and J. R. Martí, "Distribution system optimization based on a linear power-flow formulation," *IEEE Transactions on Power Delivery*, vol. 30, no. 1, pp. 25-33, Feb. 2015.
[14] H. M. Khodr, J. Martinez-Crespo, M. A. Matos *et al*., "Distribution systems reconfiguration based on OPF using benders decomposition," *IEEE Transactions on Power Delivery*, vol. 24, no. 4, pp. 2166-2176, Oct. 2009.

[15] S. Civanlar, J. J. Grainger, H. Yin *et al*., "Distribution feeder reconfiguration for loss reduction," *IEEE Transactions on Power Delivery*, vol. 3, no. 3, pp. 1217-1223, Jul. 1988.
[16] M. E. Baran and F. Wu, "Network reconfiguration in distribution systems for loss reduction and load balancing," *IEEE Transactions on Power Delivery*, vol. 4, no. 2, pp. 1401-1407, Apr. 1989.
[17] K. Prasad, R. Ranjan, N. C. Sahoo *et al*., "Optimal reconfiguration of radial distribution systems using a fuzzy mutated genetic algorithm," *IEEE Transactions on Power Delivery*, vol. 20, no. 2, pp. 1211-1213, Apr. 2005.
[18] I. I. Atteya, H. Ashour, N. Fahmi *et al*., "Radial distribution network reconfiguration for power losses reduction using a modified particle swarm optimisation," *CIRED–Open Access Proceedings Journal*, vol. 2017, no. 1, pp. 2505-2508, Jun. 2017.
[19] H. Gao, L. Wang, J. Liu *et al*., "Integrated day-ahead scheduling considering active management in future smart distribution system," *IEEE Transactions on Power Systems*, vol. 33, no. 6, pp. 6049-6061, Nov. 2018.
[20] A. M. Tahboub, V. R. Pandi, and H. H. Zeineldin, "Distribution system reconfiguration for annual energy loss reduction considering variable distributed generation profiles," *IEEE Transactions on Power Delivery*, vol. 30, no. 4, pp. 1677-1685, Aug. 2015.
[21] J. Kennedy and R. C. Eberhart, "A discrete binary version of the particle swarm algorithm," in *Proceedings of 1997 IEEE International Conference on Systems, Man, and Cybernetics, Computational Cybernetics and Simulation*, Orlando, USA, Oct. 1997, pp. 4104-4108.
[22] M. Lavorato, J. F. Franco, M. J. Rider *et al*., "Imposing radiality constraints in distribution system optimization problems," *IEEE Transactions on Power Systems*, vol. 27, no. 1, pp. 172-180, Feb. 2012.
[23] R. A. Jabr, R. Singh, and B. C. Pal, "Minimum loss network reconfiguration using mixed-integer convex programming," *IEEE Transactions on Power Systems*, vol. 27, no. 2, pp. 1106-1115, May 2012.
[24] H. Ahmadi and J. R. Martí. "Mathematical representation of radiality constraint in distribution system reconfiguration problem," *International Journal of Electrical Power & Energy Systems*, vol. 64, pp. 293-299, Jan. 2015.

Hongjun Gao received the B.S., M.S., and Ph.D. degrees in electrical engineering from Sichuan University, Chengdu, China, in 2011, 2014 and 2017, respectively. From 2015 to 2016, he was a Visiting Scholar at the Department of Electrical Engineering and Computer Science, University of Wisconsin-Milwaukee, Milwaukee, USA. He is currently an Associate Professor with the College of Electrical Engineering, Sichuan University. His research interests include active distribution system planning and operation, unit commitment, economic dispatch, distributed generation integration and multi-energy system optimization.

Wang Ma received the B.S. degree in electrical engineering from Sichuan University, Chengdu, China, in 2019, where she is currently pursuing the M.S. degree. Her research interests include distribution network operation and dynamic reconfiguration.

Yingmeng Xiang received the B. S. degree from Chongqing University, Chongqing, China, in 2010, the M.S. degree from the Huazhong University of Science and Technology, Wuhan, China, in 2013, the Ph.D. degree from University of Wisconsin-Milwaukee, Milwaukee, USA, in 2017. He is currently a Postdoc Research Associate with Iowa State University, Iowa, USA. His research interests include power distribution optimization, internet of things for power systems, smart grid reliability, cyber-physical system resiliency.

Zao Tang received the B.S. degree in electrical engineering from Sichuan University, Chengdu, China, in 2016, where she is currently pursuing the Ph.D. degree with the College of Electrical Engineering. She is a Visiting Scholar with the Electrical and Computer Engineering Department, Stevens Institute of Technology, Hoboken, USA. Her current research interests include optimal planning and operation of energy storage in power system.

Xiandong Xu received the B.Sc. and Ph.D. degrees in electrical engineering from Tianjin University, Tianjin, China, in 2009 and 2015, respectively. He is currently an Associate Professor in Tianjin University. His research interests include modelling and optimization of integrated energy systems, and operational flexibility of heat and industrial sectors.

Hongjin Pan received the B.S. degree in electrical engineering from Sichuan University, Chengdu, China, in 2019, where she is currently pursuing the M.S. degree. Her research interests include electricity market trading and comprehensive energy market game.

Fan Zhang received the B.S. degree in electrical engineering from Sichuan University, Chengdu, China, in 2019, where he is currently pursuing the M.S. degree. His research interests include distribution network trading and operation, distributed optimization and energy management.

Junyong Liu received the Ph.D. degree in electrical engineering from Brunel University, Uxbridge, UK, in 1998. He is currently a Professor with the College of Electrical Engineering, Sichuan University, Chengdu, China. He is the Director of Sichuan Province Key Smart Grid Laboratory. His current research interests include power system planning, operation, and computer applications.